Journal of Molecular Graphics and Modelling 51 (2014) 97–103

Contents lists available at ScienceDirect

Journal of Molecular Graphics and Modelling

journal homepage: www.elsevier.com/locate/JMGM

The inhibitory effect of helenalin on telomerase activity is attributed to the alkylation of the CYS445 residue: Evidence from QM/MM simulations

Zhiqiang Zhang[a,*], Liancai Xu[a], Hon-Yeung Cheung[b,**]

[a] Department of Material and Chemical Engineering, Zhengzhou University of Light Industry, Zhengzhou 450002, Henan Province, PR China
[b] Department of Biology and Chemistry, City University of Hong Kong, Hong Kong Special Administrative Region

ARTICLE INFO

Article history:
Accepted 28 April 2014
Available online 6 May 2014

Keywords:
Telomerase inhibitor
Helenalin
Sesquiterpene lactone
Anticancer
Pseudo-bond approach

ABSTRACT

Enhanced telomerase activity is a hallmark in the majority of cancer cells. Thus, understanding the interactions between telomerase and its inhibitors is fundamentally important for the development of novel anticancer drugs without severe side effects. In this study, the covalent binding of helenalin to CYS445 of telomerase (PDB ID: 3DU6) was simulated using combined quantum chemical and molecular mechanical (QM/MM) methods. The results showed that the reaction was a reversible Michael-type addition and a hydrogen bond was formed between helenalin and the side chain of LYS416 of telomerase during the reaction procedure. The LYS416 residue is vital to telomere DNA recognition by interacting with DNA base through hydrogen bonds. The alkylation of CYS445 of telomerase by helenalin may interfere with the telomere DNA recognition at the telomerase active site, thus resulting in inhibition of the enzyme activity.

1. Introduction

The telomere is associated with the longevity of life. It is located at the apex of a chromosome and protects chromosomal ends from fusion events in cells. The telomere consists of a distinct, guanine-rich quadruplex helical structure called a G-quadruplex [1], which has been shown to serve vital structural and functional roles in the chromosome [2,3]. The telomere progressively decreases in length after each round of mitotic division [4]. When the telomere length is shortened to a critical value, it can no longer form the G-quadruplex structure to protect chromosomal DNA, and the cell will undergoes senescence. Telomerase can add certain repetitive base sequences to the 3′-overhangs of telomeres [5]. This enzyme is highly expressed in a large number of cancer cell lines [6], whereas its activity is not detectable in normal cells [7]. The immortality of a large number of cancer cells may be related to the activation of telomerase, which prevents telomeres from being shortened during mitotic division. Therefore, the telomerase inhibitors may be able to treat cancers without significant side effects.

Telomerase inhibitors can be classified into different groups: first, inhibitors that target G-quadruplex telomere; second, those that target the telomere RNA template; and third, those that target the catalytic subunit of telomerase [8]. The telomerase substrate is the single-stranded telomere instead of the G-quadruplex telomere, and the G-quadruplex telomere cannot be elongated by the enzyme [9]. For the first type, selective G-quadruplex ligands can stabilize the formation and interfere telomerase activation [10]. The number of known G-quadruplex ligands has grown rapidly in recent years [11–14]. Meanwhile, the second type is based on the reverse-transcriptional property of telomerase, which requires short RNA pieces as template. Oligonucleotides are therefore good candidates for telomerase inhibition, e.g. one oligonucleotide, GRN163L, has been used as a telomerase antagonist in clinical trail [15,16]. These types of inhibitors indirectly interact with telomerase. The third type of inhibitors directly interact with the catalytic subunit of telomerase and may be superior anticancer agents in comparison to G-quadruplex ligands or oligonucleotides. However, discovering new inhibitors that target the catalytic subunit of telomerase are rarely reported partially due to the lack of understanding of the telomerase inhibitory mechanism of some compounds despite they have demonstrated inhibitory activities. For example, helenalin has been reported to exhibit a potent telomerase inhibitory effect [17]. This natural compound is involved in a large number of biological activities, most probably via its alkylation of the sulfhydryl group of biological macromolecules [17]. The α,β-unsaturated carbonyl functional group contained in helenalin tends to react with the

* Corresponding author. Tel.: +86 37186609676.
** Corresponding author.
E-mail addresses: zhangzq@zzuli.edu.cn (Z. Zhang), bhhonyun@cityu.edu.hk (H.-Y. Cheung).

http://dx.doi.org/10.1016/j.jmgm.2014.04.012
1093-3263/

sulfhydryl group through a Michael-type addition. Two such functional groups are present in helenalin: α-methylene-γ-lactone and cyclopentenone. A number of other natural compounds possess substructures similar to that of helenalin, i.e., containing an α,β-unsaturated carbonyl functional group. These compounds can also alkylate the sulfhydryl group through a Michael-type reaction [18,19].

Given the high costs of drug development, a considerable amount of effort has been made to find an effective drug from natural or semi-synthetic compounds. Natural compounds with high inhibitory effects on telomerase have been recently well-reviewed [20]. Therefore, investigating the reaction between helenalin and cysteine residues of telomerase may provide a clearer insight into the mechanism of telomerase inhibition by a number of natural products. Furthermore, understanding the mechanism of telomerase inhibition by helenalin may be valuable in discovering novel anticancer agents without severe side effects. In addition to experimental investigations, molecular modeling can also provide valuable information on the behavior of enzymatic systems, particularly when the chemical reactions are modeled using the QM/MM methods [21–25]. Thus, in this paper, the reaction between the CYS445 residue of telomerase and helenalin was simulated using the QM/MM technique. The results suggest that the alkylation of CYS445 in telomerase by helenalin may interfere with the recognition between telomere DNA and telomerase.

2. Methods

2.1. Preparation of biomolecule and helenalin

The major goal of this work is to study the reaction between helenalin and the catalytic subunit of telomerase, since the helenalin exhibited inhibitory effect on the catalytic subunit of telomerase [17]. The *Tribolium castaneum* telomerase (PDB 3DU6) [26] was used as the catalytic subunit of telomerase. The crystal structure of 3DU6 was determined to a resolution of 2.71 Å by X-ray diffraction, and is a homodimer consisting of Chains A and B. In this study, only chain A was adopted. First, chain B and all water molecules were removed from the biomolecule. Second, the reaction site was identified to be the CYS445 residue. The CYS445 was one of the most accessible cysteine residue in the chain A. What is more important is that the CYS445 residue located in the pocket of an active site which was predicted by the SYBYL SiteID module. That active site consisted of five residues, namely LEU404, TYR405, LYS416, PHE443 and SER447. Other CYS residues were not found to be in or near any active site, although other active sites were also predicted by the SYBYL SiteID module. Therefore the CYS445 residue was identified to be the reaction site. Third, the peptides outside the range from GLY391 to LYS515 were eliminated from chain A due to long distance to the reaction site, namely, the sulfur of CYS445 residue. All residues within the distance of 15 Å to the reaction site were reserved. Fourth, an acetyl group was added to the N-terminal amino acid (GLY391), an N-methyl amino was added to the C-terminal amino acid (LYS515), and all hydrogen atoms were added to the biomolecule. Finally, the biomolecule was partially optimized with all hydrogen atoms active and the other atoms frozen, using Tinker5.0 software [27] with CHARMM27 force filed [28,29]. The molecular structure of helenalin was optimized at the B3LYP/6-31G* theoretical level using G09 software package [30].

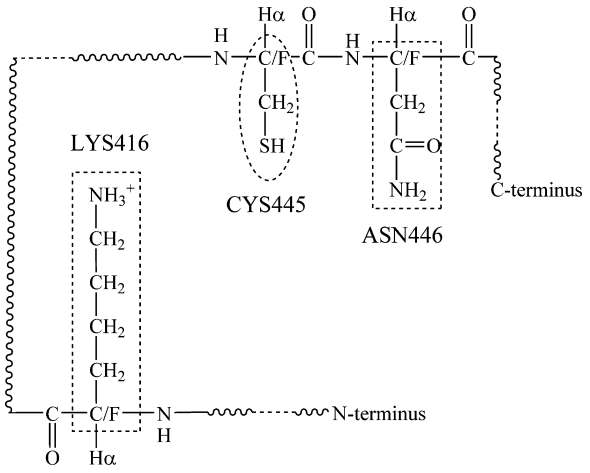

Fig. 1. Partitioning scheme of Enzyme molecule. The molecule was partitioned into four layers: QM-active (marked by dashed-ellipse), QM-background (marked by dashed-rectangles), MM-near (denoted by atom symbols outside the dashed-ellipse or dashed-rectangles) and MM-far (denoted by wave-dash-wave lines). The link atoms (denoted by C/F) were represented by pseudo-fluorines in QM calculation to produce carbon's property.

2.2. Pseudo-bond QM/MM approach

The pseudo-bond approach, developed by Yang and his coworkers [31,32], had been demonstrated as a powerful tool particularly for investigating enzymes-related reactions [33–38]. In this study, we made some minor modifications to the pseudo-bond approach to suit our needs. The modifications included geometric optimization and QM/MM energetic calculation. The modified pseudo-bond approach is described as the follows:

2.2.1. Partitioning of the QM and MM regions

The partitioning scheme of the prepared enzyme molecule was illustrated in Fig. 1. The molecule was divided into two subsystems, namely, QM and MM. QM subsystem was divided further into two layers, namely, QM-active layer (side chain of CYS445, marked by dashed-ellipse in Fig. 1) and QM-background layer (side chains of LYS416 and ASN445, marked by dashed-rectangles in Fig. 1). All small molecules (H_2O, H_3O^+ and helenalin) were treated by QM methods and belonged to QM-active layer. The MM subsystem was further divided into two layers, namely, MM-near layer (backbones of CYS445, LYS416 and ASN446, denoted by atom symbol outside the dashed-ellipse or dashed-rectangles in Fig. 1) and MM-far layer (the remaining atoms of the enzyme molecule, denoted by wave-dash-wave lines in Fig. 1). It should be mentioned that the intersection of QM and MM subsystem were the α-carbons (denoted by C/F in Fig. 1) of the three residues, namely LYS416, CYS445 and ASN446. These carbons were represented by pseudo-fluorines in QM calculations, however they participated in MM calculations in their prototype, namely α-carbons.

2.2.2. Iterative QM/MM optimization procedure

(a) QM optimization. The QM subsystem was partially optimized with the QM-background layer fixed. The optimization used the electronic embedding scheme in which the MM atoms were represented by point charges. In this case, only the MM-far atoms were represented by point charges. However, the point charge of MM-near atoms were set to zero in order to avoid the overpolarization of the covalent bond at the QM/MM interface because a point charge assigned to the MM nucleus does not provide a good approximation for the smeared distribution of charge density at such short distance. The alpha carbons of CYS445, LYS416 and ASN446 were treated as the link atoms, and represented

by pseudo-fluorines with effective core potentials. The optimization was carried out at the B3LYP/3-21G theoretical level using a quasi-Newton minimizer in internal coordinates with G09 software packages.

(b) MM optimization. The entire molecule was optimized with the QM-active layer fixed until convergence using the truncated Newton method in Cartesian coordinates with the CHARMM27 force field. The atomic charges for QM-active and QM-background atoms were updated by the Mulliken charges obtained from the preceded QM optimization. In the QM calculation, the sum of the Mulliken charges over all QM atoms was 1.0 due to the presence of the quaternary ammonium cation in the QM subsystem. On the other hand, CHARMM27 force field assigned a partial charge of 0.07 to the α-carbon of a residue, and a formal charge, e.g. 0, +1, −1, to the side chain of a residue. The value of the formal charge was determined by the type and ionization state of the residue. The sum of the defined partial charges was 1.21 over all atoms in the QM-active and QM-background layers, and not equal to the sum of Mulliken charges of those atoms. Therefore the total charge of the enzyme molecule changed after the updating of the partial charge of QM atoms. In order to keep the total charge of the entire enzyme consistent, a partial charge of 0.16 was assigned to the hydrogen which connected with the α-carbon and was denoted by Hα in Fig. 1, whereas the original defined partial charge of that type of hydrogen was 0.09 in the CHARMM27 force field. The MM optimizations were performed using Tinker5.0 packages.

(c) Steps a and b were repeated until both meet the convergence criteria at the same geometry.

2.2.3. Convergence criteria in QM/MM calculations

The convergence criterion for the optimization of the MM and QM-inactive subsystems was that the final rms gradient should be below 0.1 kcal mol^{-1} Å^{-1}. Two convergence criteria, namely, loose and normal, were used for the optimization of QM subsystems. The loose convergence criteria are as follows: maximum gradient 0.002500 a.u., rms gradient 0.001667 a.u., maximum displacement 0.010000 a.u., rms displacement 0.006667 a.u. (gradient 0.00030 a.u. is 0.35 kcal mol^{-1} Å^{-1}). The normal convergence criteria are as follows: maximum gradient 0.00045 a.u., rms gradient 0.00030 a.u., maximum displacement 0.0018 a.u., rms displacement 0.0012 a.u. The normal convergence criteria were the default criteria in the G09 package. The normal criteria were used for the geometric optimization of the stationary points in the potential energy surface, whereas the loose criteria were used for the geometric optimization of the points along the minimum energy path.

2.2.4. The potential energy of the QM/MM system

When the QM/MM optimization was completed, the potential energy of the entire system was recalculated based on the optimized geometry at a more precise theoretical level, as follows:

$$E_{total} = E_{qm}(QM) + E_{mm}(MM) + E_{qm/mm}\left(QM/MM\right) \quad (1)$$

where the E_{qm} is the quantum chemical energy of the QM subsystem, including both QM-active and QM-inactive subsystem, and the E_{mm} is the molecular mechanical energy of the MM subsystem. The $E_{qm/mm}$ is the interaction between the QM and MM subsystems consists of three terms, which are expressed as follows:

$$E_{qm/mm}\left(QM/MM\right) = E_{\text{electronics}}\left(QM/MM\right) + E_{vdw}\left(QM/MM\right) + E_{MM\text{-bonded}}\left(QM/MM\right) \quad (2)$$

where $E_{MM\text{-bonded}}$ is the molecular mechanics energies of bond stretching, angle bending, and torsional terms, which involve at least one atom from the MM subsystem and one from the QM subsystem. E_{mm}(MM) and $E_{qm/mm}$(QM/MM) were calculated using the Tinker5.0 packages and CHARMM27 force fields. E_{qm}(QM) was calculated at the B3LYP/6-31G* theoretical level, and the basis set superposition error was corrected by means of counterpoise method [39]. The QM calculation was performed in the presence of the MM subsystem by including terms that describe the electrostatic interaction between QM and MM as one-electron operators that enter the QM Hamiltonian. The CHARMM27 force fields developed extensive sets of atomic-centered partial charge. Thus, the MM atoms were represented by atomic-centered partial point charges in the effective QM Hamiltonian. Given that the $E_{\text{electronics}}$(QM/MM) term in $E_{qm/mm}$(QM/MM) has been calculated using MM method, the contribution of electrostatic interactions between the QM and MM subsystem to the QM energy should be subtracted from the QM calculation. Yang et al. [31] pointed out that the terms for the electrostatic interactions between the QM and MM subsystem in the effective Hamiltonian approximate the sum of the coulombic energies, which are expressed as

$$E^{qm}_{\text{electronics}}\left(QM/MM\right) \approx \sum_{\alpha\in QM,\beta\in MM} \frac{Q^*_\alpha q_\beta}{r_{\alpha\beta}} \quad (3)$$

where Q^*_α is the electrostatic potential fitted (ESP) [40,41] charge on the QM atom α. By using the assumption described as Eq. (3), the terms of electrostatic interactions between QM and MM were conveniently subtracted from the effective Hamiltonian in the QM calculations. Here, the Mulliken atomic charges instead of ESP charges were adopted to calculate electrostatic interactions term.

3. Results and discussion

3.1. Geometric optimization and structure overview of the intermediate and product

The reaction between the CYS445 residue of telomerase (**Enz-SH**) and helenalin is a Michael-type addition (Scheme 1). The first step was the deprotonation of the sulfhydryl group of the CYS445 residue in telomerase to result in the more active thiolate form (**Enz-S$^-$**) in the Michael-type addition. The second step was the formation of the intermediate (**IM**), in which a new covalent bond formed between CYS445 and helenalin. The third step was the protonation of **IM** to yield the product (**Prod**). **IM** came into contact with reactant and product. Its geometry was essential for determining the reaction path. The **IM** geometry was therefore first optimized. Fig. 2a–c showed the optimized geometry of **IM**, helenalin and the QM subsystem of **IM**, respectively. Two potentially reactive sites, namely, **C^1** and **C′** (Fig. 2b), occurred at helenalin

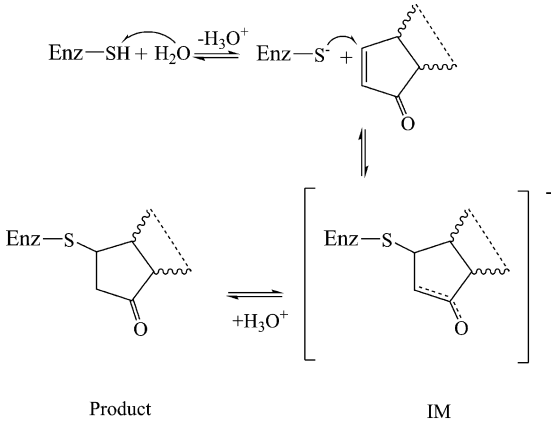

Scheme 1. Mechanism of the Michael-type addition between the CYS445 residue of telomerase and helenalin.

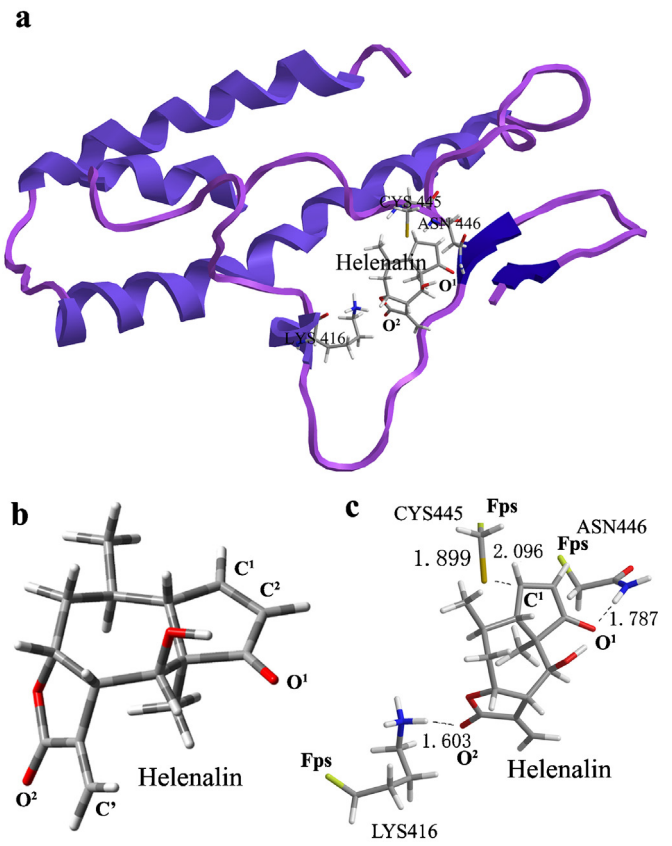

Fig. 2. (a) Entire molecular geometry of **IM** obtained from iterative QM/MM optimization. The MM subsystem is represented by the tube and colored by the secondary structure. The QM subsystem is represented by sticks. Hydrogen bonds between helenalin and telomerase are represented by dashed lines. (b) Optimized geometry of helenalin. Atoms are colored by type: gray for carbon, white for hydrogen, and red for oxygen. (c) Optimized geometry of the QM subsystem of **IM**. Atoms are colored by type: gray for carbon, white for hydrogen, red for oxygen, blue for nitrogen, and light blue for link atom.

for the Michael-type reaction. The $\mathbf{C^1}$ atom was the β-carbon of the cyclopentenone subsystem of helenalin, whereas the $\mathbf{C'}$ atom was the β-carbon of the α-methylene-γ-lactone subsystem of helenalin. The activity of the cyclopentenone structure is generally higher than that of α-methylene-γ-lactone when both are present in a molecule, as reported in helenalin [42,43]. Therefore, the $\mathbf{C^1}$ of helenalin was considered as the reactive site in the current study. The initial geometric model of **IM** was prepared by linking the $\mathbf{C^1}$ atom of helenalin to sulfur atom of the CYS445 of the prepared enzyme molecule. The model was then subjected to iterative QM/MM optimization using the normal convergence criteria.

In **IM**, the main interactions between the enzyme and helenalin consisted of three bond, namely, a covalent bond and two hydrogen bonds (shown in Fig. 2c). The covalent bond was the newly formed S—C single bond with a bond length of 2.096 Å. On the other hand, the S—C bond length of the CYS445 side chain was 1.899 Å. The newly formed S—C bond was therefore a relatively weak one. In **IM**, the carbonyl $\mathbf{O^1}$ of helenalin was near to the ASN446 side chain, while the carbonyl $\mathbf{O^2}$ of helenalin was near to the tip of the LYS416 side chain. The distance between the amide hydrogen of the ASN446 side chain and $\mathbf{O^1}$ of helenalin was 1.787 Å, and the distance between the amino hydrogen of the LYS416 side chain and $\mathbf{O^2}$ of helenalin was 1.603 Å. Both values fall within the hydrogen bond distance.

The **Prod** was the protonated **IM**. The initial geometry of **Prod** was constructed based on the optimized geometry of **IM** by connecting an H to the $\mathbf{C^2}$ of helenalin. The geometry of **Prod** was also subject to iterative QM/MM optimization with normal convergence criteria. Fig. 3a showed the optimized geometry of **Prod**'s QM subsystem. The distance between $\mathbf{C^1}$ and **S** was 1.916 Å which indicated that the S—C between CYS445 and helenalin became stronger after the protonation, because the bond length of that S—C bond in **IM** was 2.096 Å which was 0.02 Å longer than **Prod**. The two hydrogen bonds between helenalin and the enzyme occurred in **IM** were also found in **Prod**. The bond length of the hydrogen bond between ASN446 and helenalin was 1.988 Å, and the bond length of the hydrogen bond between LYS416 and helenalin was 1.599 Å. The two hydrogen bonds were present during the reaction procedure between CYS445 and helenalin (details shown in Supplementary Information.).

3.2. Minimum energy path for the second step

The second step of the reaction was the formation of S—C single bond between the CYS445 sulfur and the $\mathbf{C^1}$ of helenalin. The minimum energy path for this step was determined using the coordinate-driving method, which involves stepping along a proposed reaction coordinate and performing the energy minimization with respect to the remaining coordinates. Here the reaction coordinate was defined as the distance between **S** of CYS445 residue and $\mathbf{C^1}$ of helenalin. The optimized geometry of **IM** was used as the starting point. The reverse path was first mapped by increasing the value of the reaction coordinate by 0.05 Å (before the S—C bond length was less than 2.35 Å) or 0.1 Å (after the bond length exceeded 2.35 Å) until the value of reaction coordinate reaching 3.65 Å. The forward reaction path was minimized by decreasing the value of the reaction coordinates in a similar manner by using the end point

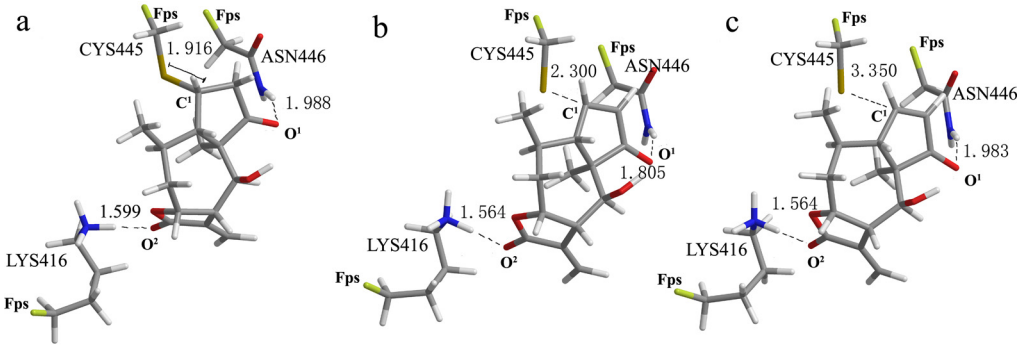

Fig. 3. (a) The QM geometry structure of **Prod**. (b) The QM geometry of **TS**. (c) The QM geometry of the QM subsystem of **State1**. Atoms are colored by type: gray for carbon, white for hydrogen, red for oxygen, blue for nitrogen, and light blue for link atom F_{ps}. (For interpretation of the references to color in this figure legend, the reader is referred to the web version of this article.)

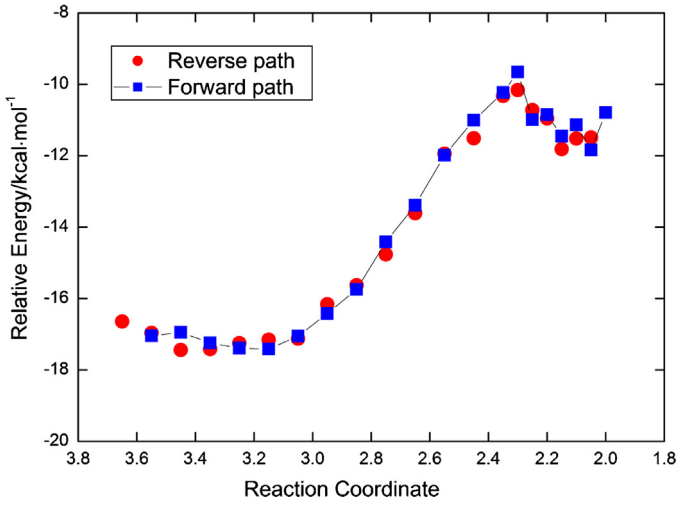

Fig. 4. The minimum energy path for the second step of the Michael-type reaction between telomerase CYS445 and helenalin. The reaction coordinate was defined as the distance between the CYS445 sulfur and $\mathbf{C}^1$ of helenalin.

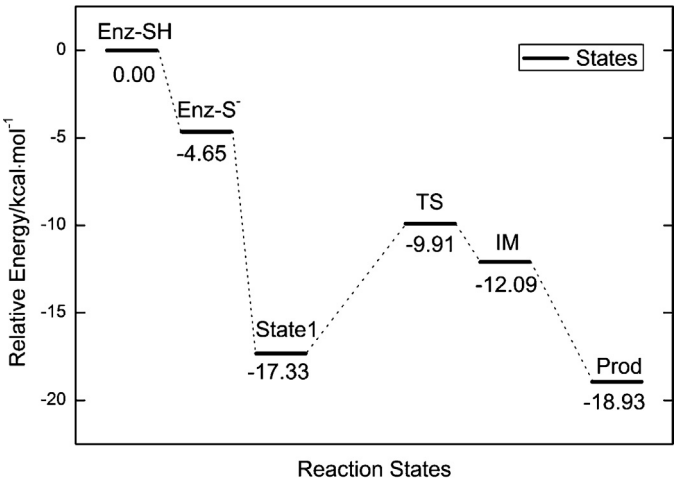

Fig. 5. Potential energy surface of the Michael-type reaction between the CYS445 residue of telomerase and helenalin. The energy of **Enz-SH** was the sum of the energies of telomerase, helenalin and water, and was defined as the reference. The energy of **Enz-S**$^-$ was the sum of the energies of the deprotonated telomerase (CYS445 sulfhydryl deprotonated), helenalin, and protonated water. The energy of **State1** was the sum of the energies of protonated water and the total energy of the complex of deprotonated telomerase and helenalin. The energy of **TS** was the sum of the energies of protonated water and the total energy of the transition state. The energy of **IM** was the sum of the energies of protonated water and the total energy of the intermediate. The energy of **Prod** was the sum of the energies of the final adduct of the Michael-type reaction and the energy of water.

of reverse path as its starting point. As shown in Fig. 4, the minimum energy paths were smooth, and the two directions, namely, forward and reverse, along the path were similar to each other.

The coordinate-driving method is also practical for locating the transition state because the Hessian of the potential energy surface based method is not suitable for systems involving macromolecules, such as the system encountered in this study. The geometry with the maximum value along the minimum energy path is a good approximation of the transition state geometry [32]. A local maximum was found in each path. They both located at the reaction coordinate of 2.30 Å. Fig. 3b showed the geometry of the QM subsystem of the approximate transition state (**TS**) which was determined from the forward path. In the **TS**, a hydrogen bond between LYS416 and $\mathbf{O}^2$ of helenalin was found, and the bond length was 1.564 Å. At the same time, a hydrogen bond between ASN446 and $\mathbf{O}^1$ of helenalin was found, and the bond length was 1.805 Å.

A local minimum was also found near the left end of each path. However, the local minimums in the reverse and forward path located at different reaction coordinates. The local minimum in the average of the reverse and forward path located at the reaction coordinate of 3.35 Å. This state was named by **State1**, and referred to the complex of **Enz-S**$^-$ and helenalin. Fig. 3c showed the geometry of QM subsystem of **State1** which was determined from the forward minimum energy path. Two hydrogen bonds also occurred in **State1**. The bond length was 1.564 Å for the hydrogen bond between LYS416 and helenalin, while the bond length was 1.983 Å for the hydrogen bond between ASN446 and helenalin.

According to the minimum energy path, the activation energy for S—C bond formation was approximately 7.4 kcal mol^{-1}.

3.3. Overview of the reaction potential energy surface

The reaction potential energy surface was shown in Fig. 5. The energy of **Enz-SH** state was calculated as the sum of the energies of **Enz-SH**, helenalin, and H_2O. Given that the reaction occurred in an aqueous environment in which no protons exists, a molecule of water was considered as the proton receptor in the reaction. The energy of this state was defined as the reference which was set to 0.00 kcal mol^{-1}. Energy of other states was the relative energy with respect to the reference, and calculated according to the law of conservation of matter. The relative energy of **Enz-S**$^-$ state was −4.65 kcal mol^{-1}. It indicated that the deprotonation of sulfhydryl group of CYS445 was a spontaneous process. The relative energy of **State1** was −17.33 kcal mol^{-1}, which indicated that the formation of the complex of **Enz-S**$^-$ and helenalin was also a spontaneous process and it will release about 12.7 kcal mol^{-1} of heat. The conversion from **State1** to **IM** involved the formation of covalent bond. It is an endothermic process which required about 5.2 kcal mol^{-1} of energy to form **IM** and about 7.4 kcal mol^{-1} of energy to conquer the energy barrier. The relative energy of **Prod** was −18.93 and the conversion from **IM** to **Prod** was a exothermic and spontaneous process. The process would release about 6.8 kcal mol^{-1} of heat. Although the relative energy of **Prod** was about 1.6 kcal mol^{-1} lower than that of **State1**, the reverse conversion from **Prod** to **State1** was still allowed in thermodynamics. Therefore, the conversion from **State1** to **Prod** was reversible. However the dissociation of **State1** into **Enz-S**$^-$ and helenalin was not thermodynamically favorable.

3.4. Mechanism of telomerase inhibition by helenalin

The telomerase protein consists of four domains, namely, the RNA-binding domain (TRBD), finger domain, palm domain, and thumb domain. The finger domain is implicated in nucleotide binding and processivity [26,44,45]. The palm domain contains the active site of the enzyme, whereas the thumb domain is involved in DNA binding and processivity [26,45,46]. The four domains were organized into a ring configuration to accommodate the RNA and DNA hybrid bases [45]. The interaction between DNA and the thumb loop included LYS416 side chain, which was a reserved residue in the thumb domain, and several other hydrophilic residues. The recognition between the hybrid double helix and the enzyme was facilitated by the hydrogen bond between the LYS416 side chain and the DNA backbone [45]. The CYS445 side chain extended toward the center of the ring at the point that contact between the palm domain and the TRBD domain. In addition, the distance between CYS445 and LYS416 was within the molecular length of helenalin. According to the QM/MM study, the CYS445 residue tends to be alkylated by helenalin through Michael type reaction. A hydrogen bond between helenalin and the

LYS416 side chain was formed at the reactants complex, namely **State1**. That hydrogen bond was retained in the following reaction process. This hydrogen bond interfered with the interaction between the LYS416 side chain and the DNA base. Moreover, the alkylation of CYS445 by helenalin disrupted the interior profile of the ring structure of telomerase by reducing the ring capacity. As a result, the binding of the RNA/DNA hybrid in telomerase was disturbed, and the telomerase activity was inhibited.

4. Conclusions

A simulation of the reaction between CYS445 of telomerase and helenalin was performed using QM/MM calculations. The reaction was a typical Michael-type reaction. In the first step, the sulfhydryl group of the CYS445 residue was spontaneously deprotonated to yield the thiolate form which is more active in the reaction. The CYS445-deprotonated telomerase and helenalin prefered to bind with each other through hydrogen bonds to form reactants complex. The formation of reactants complex released about 12.7 kcal mol^{-1} of energy. In the second step, the cyclopentenone group of helenalin was attacked by the thiolate group of CYS445 residue to form an intermediate. In the final step, the intermediate was spontaneously protonated to yield the addition product. The second step of the reaction was the rate-determining step in which about 7.4 kcal mol^{-1} of energy was required to conquer the energy barrier. The total energy for the Michael-type reaction was −18.93 kcal mol^{-1}. The results indicate that the CYS445 residue of telomerase was readily alkylated by helenalin through a Michael-type reaction.

The LYS416 reportedly played an important role in the recognition between telomerase and its DNA substrate, because the hydrophilic side chain of LYS416 tend to form hydrogen bond with DNA base to facilitate the binding of DNA at the active site of telomerase. In the process of the reaction between CYS445 of telomerase and helenalin, a hydrogen bond was formed between LYS416 and helenalin in the reactants complex. The hydrogen bond was retained in the following reaction process. Although the product could reversibly convert to the reactants complex, the dissociation of the complex into enzyme and helenalin was not thermodynamically favorable. Therefore, the hydrogen bond could be formed between LYS416 and helenalin as long as helenalin occurred in the CYS445 site no matter whether they covalently bond with each other or not. The following conclusions were thus drawn: (1) a hydrogen bond between the LYS416 side chain of telomerase and helenalin was formed during the alkylation of CYS445 by helenalin through a Michael-type addition; and (2) the recognition of telomeres at the telomerase active site was disrupted by the aforementioned hydrogen bond, which result in the inhibition of enzyme activity.

Acknowledgement

This work is financially supported by National Natural Science Foundation of China (U1204209) and the Doctoral Funds of Zhengzhou University of Light Industry (BSJJ-2011013 and BSJJ-2011012).

Appendix A. Supplementary data

Supplementary data associated with this article can be found, in the online version, at http://dx.doi.org/10.1016/j.jmgm.2014.04.012.

References

[1] R.K. Moyzis, J.M. Buckingham, L.S. Cram, M. Dani, L.L. Deaven, M.D. Jones, et al., A highly conserved repetitive DNA-sequence, (Ttaggg)N, present at the telomeres of human-chromosomes, P. Natl. Acad. Sci. U. S. A. 85 (1988) 6622–6626.
[2] W.H. Chai, Q. Du, J.W. Shay, W.E. Wright, Human telomeres have different overhang sizes at leading versus lagging strands, Mol. Cell. 21 (2006) 427–435.
[3] V.L. Makarov, Y. Hirose, J.P. Langmore, Long G tails at both ends of human chromosomes suggest a C strand degradation mechanism for telomere shortening, Cell 88 (1997) 657–666.
[4] C.B. Harley, A.B. Futcher, C.W. Greider, Telomeres shorten during aging of human fibroblasts, Nature 345 (1990) 458–460.
[5] G.B. Morin, The human telomere terminal transferase enzyme is a ribonucleoprotein that synthesizes ttaggg repeats, Cell 59 (1989) 521–529.
[6] N.W. Kim, M.A. Piatyszek, K.R. Prowse, C.B. Harley, M.D. West, P.L.C. Ho, et al., Specific association of human telomerase activity with immortal cells and cancer, Science 266 (1994) 2011–2015.
[7] E. Hiyama, K. Hiyama, Telomere and telomerase in stem cells, Br. J. Cancer. 96 (2007) 1020–1024.
[8] A. De Cian, L. Lacroix, C. Douarre, N. Temime-Smaali, C. Trentesaux, J.F. Riou, et al., Targeting telomeres and telomerase, Biochimie 90 (2008) 131–155.
[9] A.M. Zahler, J.R. Williamson, T.R. Cech, D.M. Prescott, Inhibition of telomerase by G-Quartet DNA structures, Nature 350 (1991) 718–720.
[10] J.H. Tan, L.Q. Gu, J.Y. Wu, Design of selective G-quadruplex ligands as potential anticancer agents, Mini-Rev. Med. Chem. 8 (2008) 1163–1178.
[11] A. Arola, R. Vilar, Stabilisation of G-quadruplex DNA by small molecules, Curr. Top. Med. Chem. 8 (2008) 1405–1415.
[12] N.W. Luedtke, Targeting G-quadruplex DNA with small molecules, Chimia 63 (2009) 134–139.
[13] D.L. Ma, C.M. Che, S.C. Yan, Platinum(II) complexes with dipyridophenazine ligands as human telomerase inhibitors and luminescent probes for G-quadruplex DNA, J. Am. Chem. Soc. 131 (2009) 1835–1846.
[14] M.C. Nielsen, T. Ulven, Macrocyclic G-quadruplex ligands, Curr. Med. Chem. 17 (2010) 3438–3448.
[15] Z.G. Dikmen, G.C. Gellert, S. Jackson, S. Gryaznov, R. Tressler, P. Dogan, et al., In vivo inhibition of lung cancer by GRN163L: a novel human telomerase inhibitor, Cancer Res. 65 (2005) 7866–7873.
[16] M.W. Djojosubroto, A.C. Chin, N. Go, S. Schaetzlein, M.P. Manns, S. Gryaznov, et al., Telomerase antagonists GRN163 and GRN163L inhibit tumor growth and increase chemosensitivity of human hepatoma, Hepatology 42 (2005) 1127–1136.
[17] P.R. Huang, Y.M. Yeh, T.C.V. Wang, Potent inhibition of human telomerase by helenalin, Cancer Lett. 227 (2005) 169–174.
[18] Z. Zhang, G.K.-L. Chan, J. Li, W.-F. Fong, H.-Y. Cheung, Molecular interaction between andrographolide and glutathione follows second order kinetics, Chem. Pharm. Bull. 56 (2008) 1229–1233.
[19] Z.Q. Zhang, R.K.K. Chow, H.W. Zhou, J.L. Li, H.-Y. Cheung, An ab initio study on the structure–cytotoxicity relationship of terpenoid lactones based on the Michael reaction between their pharmacophores and L-cysteine-methylester(-1), J. Theor. Comput. Chem. 7 (2008) 347–356.
[20] J.L.Y. Chen, J. Sperry, N.Y. Ip, M.A. Brimble, Natural products targeting telomere maintenance, MedChemComm 2 (2011) 229–245.
[21] Q.Q. Hou, J.H. Wang, J. Gao, Y.J. Liu, C.B. Liu, QM/MM studies on the catalytic mechanism of phenylethanolamine N-methyltransferase, BBA-Proteins Proteomics 1824 (2012) 533–541.
[22] J.L. Liu, C.C. Zhang, D.G. Xu, QM/MM study of catalytic mechanism of Xylanase Cex from *Cellulomonas fimi*, J. Mol. Graph. Model. 37 (2012) 67–76.
[23] G. Moraes, V. Azevedo, M. Costa, A. Miyoshi, A. Silva, V. da Silva, et al., Homology modeling, molecular dynamics and QM/MM study of the regulatory protein PhoP from *Corynebacterium pseudotuberculosis*, J. Mol. Model. 18 (2012) 1219–1227.
[24] A.G. Taranto, P. Carvalho, M.A. Avery, QM/QM studies for Michael reaction in coronavirus main protease (3CL(Pro)), J. Mol. Graph. Model. 27 (2008) 275–285.
[25] J.H. Wang, Q.Q. Hou, L.H. Dong, Y.J. Liu, C.B. Liu, QM/MM studies on the glycosylation mechanism of rice BGlu1 beta-glucosidase, J. Mol. Graph. Model. 30 (2011) 148–152.
[26] A.J. Gillis, A.P. Schuller, E. Skordalakes, Structure of the *Tribolium castaneum* telomerase catalytic subunit TERT, Nature 455 (2008) 633–636.
[27] J.W. Ponder, Tinker, Software Tools for Molecular Design, Version 5.0, 2010.
[28] N. Foloppe, A.D. MacKerell, All-atom empirical force field for nucleic acids: I. Parameter optimization based on small molecule and condensed phase macromolecular target data, J. Comput. Chem. 21 (2000) 86–104.
[29] A.D. MacKerell, D. Bashford, M. Bellott, R.L. Dunbrack, J.D. Evanseck, M.J. Field, et al., All-atom empirical potential for molecular modeling and dynamics studies of proteins, J. Phys. Chem. B 102 (1998) 3586–3616.
[30] M.J. Frisch, G.W. Trucks, H.B. Schlegel, G.E. Scuseria, M.A. Robb, J.R. Cheeseman, et al., GAUSSIAN 09 Revision D.01, Gaussian, Inc., Wallingford, CT, 2013.
[31] Y.K. Zhang, T.S. Lee, W.T. Yang, A pseudobond approach to combining quantum mechanical and molecular mechanical methods, J. Chem. Phys. 110 (1999) 46–54.
[32] Y.K. Zhang, H.Y. Liu, W.T. Yang, Free energy calculation on enzyme reactions with an efficient iterative procedure to determine minimum energy paths on a combined ab initio QM/MM potential energy surface, J. Chem. Phys. 112 (2000) 3483–3492.

[33] G.A. Cisneros, H.Y. Liu, Y.K. Zhang, W.T. Yang, Ab initio QM/MM study shows there is no general acid in the reaction catalyzed by 4-oxalocrotonate tautornerase, J. Am. Chem. Soc. 125 (2003) 10384–10393.
[34] T. Hori, H. Takahashi, S.I. Furukawa, M. Nakano, W.T. Yang, Computational study on the relative acidity of acetic acid by the QM/MM method combined with the theory of energy representation, J. Phys. Chem. B 111 (2007) 581–588.
[35] H. Hu, A. Boone, W.T. Yang, Mechanism of OMP decarboxylation in orotidine 5′-monophosphate decarboxylase, J. Am. Chem. Soc. 130 (2008) 14493–14503.
[36] X.Q. Hu, H. Hu, J.A. Melvin, K.W. Clancy, D.G. McCafferty, W.T. Yang, Autocatalytic intramolecular isopeptide bond formation in Gram-positive bacterial pili: a QM/MM simulation, J. Am. Chem. Soc. 133 (2011) 478–485.
[37] J.M. Parks, H. Hu, J. Rudolph, W.T. Yang, Mechanism of Cdc25B phosphatase with the small molecule substrate p-nitrophenyl phosphate from QM/MM-MFEP calculations, J. Phys. Chem. B 113 (2009) 5217–5224.
[38] J.M. Parks, R.K. Kondru, H. Hu, D.N. Beratan, W.T. Yang, Hepatitis C virus NS5B polymerase: QM/MM calculations show the important role of the internal energy in ligand binding, J. Phys. Chem. B 112 (2008) 3168–3176.
[39] S.F. Boys, F. Bernardi, Calculation of small molecular interactions by differences of separate total energies – some procedures with reduced errors, Mol. Phys. 19 (1970) 553–566.
[40] B.H. Besler, K.M. Merz, P.A. Kollman, Atomic charges derived from semiempirical methods, J. Comput. Chem. 11 (1990) 431–439.
[41] U.C. Singh, P.A. Kollman, An approach to computing electrostatic charges for molecules, J. Comput. Chem. 5 (1984) 129–145.
[42] A.C. Beekman, H.J. Woerdenbag, W. van Uden, N. Pras, A.W.T. Konings, H.V. Wikstrom, et al., Structure – cytotoxicity relationships of some helenanolide-type sesquiterpene lactones, J. Nat. Prod. 60 (1997) 252–257.
[43] T.J. Schmidt, Helenanolide-type sesquiterpene lactones 3. Rates and stereochemistry in the reaction of helenalin and related helenanolides with sulfhydryl containing biomolecules, Bioorg. Med. Chem. 5 (1997) 645–653.
[44] D. Bosoy, N.F. Lue, Functional analysis of conserved residues in the putative “finger” domain of telomerase reverse transcriptase, J. Biol. Chem. 276 (2001) 46305–46312.
[45] M. Mitchell, A. Gillis, M. Futahashi, H. Fujiwara, E. Skordalakes, Structural basis for telomerase catalytic subunit TERT binding to RNA template and telomeric DNA, Nat. Struct. Mol. Biol. 17 (2010) 513–518.
[46] S. Hossain, S. Singh, N.F. Lue, Functional analysis of the C-terminal extension of telomerase reverse transcriptase – a putative “Thumb” domain, J. Biol. Chem. 277 (2002) 36174–36180.